Hybrid sensors using laser targeting

Riza, Nabeel, Ghauri, Farzan, Perez, Frank

Nabeel A. Riza, Farzan Ghauri, Frank Perez, "Hybrid sensors using laser targeting," Proc. SPIE 6189, Optical Sensing II, 618905 (22 April 2006); doi: 10.1117/12.663118

SPIE.

Event: SPIE Photonics Europe, 2006, Strasbourg, France

Hybrid Sensors using Laser Targeting

Nabeel A. Riza [1,2], Farzan Ghauri [2], and Frank Perez [1]
[1] Nuonics, Inc.
1025 S. Semoran Blvd., Suite 1093, Winter Park, FL 32792, USA.
[2] College of Optics-CREOL, University of Central Florida
4000 Central Florida Blvd., Orlando, FL 32816-2700

ABSTRACT

Proposed, to the best of our knowledge, is the first extreme environment wireless all-in-one hybrid temperature plus pressure sensor using a remoted thick single crystal Silicon Carbide chip within a pressurized capsule. Analysis and experiments are reported for the pressure aspect of the sensor for pressures up-to 40 atms.

Keywords: Optical sensors, temperature sensor, pressure sensor, extreme environments

1. INTRODUCTION

Optical sensors are beginning to play an important role in industrial sensing scenarios where the natural remoting capability of the optical fiber is a dominant feature of the sensing system [1]. In particular, temperature and pressure sensors are required for extreme environment applications such as fossil-fuel based power generation systems. Recently, a hybrid fiber-freespace optics approach to sensing was put forth that exploits both the fiber-based remoting capability and the minimally invasive nature of laser targeted light beams incident on specific sensing frontend chips [2-4]. Specifically for harsh environments, the use of the single crystal silicon carbide (SiC) has been suggested to enable temperature, pressure, and gas species sensing. Data from the recently demonstrated SiC sensor has shown successful temperature measurements from room temperature to 1000°C, with pressures from 1 to 50 bars. SiC chip refractive index and thickness measurements up-to 1000°C have also been possible with nanometer equivalent sensitivities [5].

This paper introduces a novel wireless optical sensor design that can be used for measuring both temperature and pressure, hence realizing a hybrid temperature plus pressure sensor. Sensing is accomplished by monitoring the local and global spatial optical properties of the freespace laser beam retro-reflected from the SiC optical chip placed in a sealed capsule interconnected to the environment undergoing temperature and/or pressure changes. Specifically, environmental conditions imposed on the chip cause optical and mechanical properties of the chip to change such as changes in chip refractive index and global thickness. By detecting these chip localized and global (i.e., over the entire illuminated chip region) optical and physical changes, the given extreme environmental conditions can be deduced.

This paper will focus on the pressure measurement aspect of the proposed hybrid temperature+pressure sensor. A detailed prior art citation for pressure sensors is given to put the proposed innovation in perspective. It is highlighted that these prior-art electronic and optical sensor designs require extreme environment protection packaging of the sensing element to prevent sensing element damage, thus making a very challenging sensor design. In addition, the sensor now becomes an in-direct reader of the extreme environment conditions as it is not in direct contact with the conditions. In the proposed hybrid sensor, the SiC chip solves these prior-art problems as the SiC material itself is the direct sensing element as well as the packaging window. Preliminary experiments from the proposed pressure sensor are presented including demonstrated pressure measurement ranges and sensitivity, and comparison with theoretical models for chip mechanical deformation. Issues related to sensor packaging and controls are discussed.

Optical Sensing II, edited by Brian Culshaw, Anna G. Mignani, Hartmut Bartelt, Leszek R. Jaroszewicz,
Proc. of SPIE Vol. 6189, 618905, (2006) · 0277-786X/06/$15 · doi: 10.1117/12.663118

2. PRESSURE SENSORS: A SURVEY

Pressure sensors have been built by utilizing the variation in the resistance or capacitance of a device under pressures. Prototype silicon carbide (SiC) high temperature piezoresistive pressure sensors were batch-fabricated at the NASA John Glenn Research Center by producing the diaphragms using a chemical micromachining process, and the sensors showed promise and were demonstrated to operate up to 500ºC [6]. Okojie et al. [7] fabricated and tested piezoresistive pressure sensors with full scale output 40.66 and 20.03 mV at 23ºC and 500ºC, respectively, at 1000 psi (or 68 atm). Ziermann et al. [8] used Silicon Carbide on Insulator (SiCOI) to create a piezoresistive pressure sensors and tested its operation between room temperature and 500ºC. They reported the sensitivity of the device to be 20.2 μV/V·kPa at room temperature. Since these SiC sensors are based on the principle of piezoresistance, micropipe defects in SiC negatively impact performance. Further research is necessary to harness the full potentials of SiC as efficient high temperature pressure sensors surpassing the capability of silicon-based sensors. Attempts have also been made to make SiC membrane optical MEMS fiber-optic pressure sensors using Sapphire fibers [9]. Here, performances are shown for relatively low pressures (e.g., 20 psi) using the thin SiC membranes. Moreover, all these SiC MEMS pressure sensors are not wireless passive devices as proposed for our optical sensor. In otherwords, electronic power and processing is done on chip or via remoted fiber (e.g., Sapphire fiber that is limited by multi-modal optical noise) that is also being simultaneously exposed to the changing high pressure and temperature environment. In effect, all the processing in the chip (plus fiber connection for the optical MEMS case) must withstand the environmental effects. Works on producing a wireless pressure sensor includes references [10-12]. These highlighted sensors require on-chip power plus electronics and contacts that are non-robust to high temperatures. Another design proposed is passive, nevertheless, it presently has limitations in temperature (< 400 ºC)and pressure (< 7 bars) ranges of operations [13].

In silicon technology, p-n junction-isolated piezoresistors are used as pressure sensors for temperatures less than 175ºC, and silicon-on-insulator (SOI) sensors for temperatures up to 500ºC. Other techniques have also been investigated to measure pressure. Leading fiber-optic sensors such as using fiber Fabry-Perot interference or in-fiber Bragg Gratings with wavelength-based processing by use of the fiber wire for light delivery and light return do not form the needed wireless pressure sensor [14-21]. Optically reflective [22] and interferometric [23-26] techniques have also been investigated. The interferometric techniques were based on Fabry-Pérot interferometer/cavity formed by etching a glass substrate or the tip of an optical fiber and enclosing the etched volume with a silicon diaphragm. The materials in these optical devices were glass and silicon which will melt at the high temperature environment in fossil fuel applications. Recently further work in optical pressure sensor has been reported, but all have their limitations due to the exposure of their non-robust sensing element and/or their connecting fibers in the extreme power generation systems environment. These are listed in references [27-34]. All these fiber-based optical pressure sensors are non-wireless designs.

3. PROPOSED HYBRID TEMPERATURE-PRESSURE SENSOR- RATIONALE AND DESIGN

Generation of clean energy is an important global concern [35]. Early fossil fuel power generation system designs show improved conversion efficiencies and lower emissions when operating at extreme temperatures (> 1500 °C) and pressures (> 50 atms, e.g., 400 atm) [36]. Apart from meeting temperature and pressure range requirements, sensors need to be long lived and reliable. Most importantly, these sensors need to survive extreme chemical conditions, e.g., acids, hot gases, molten metals, and sludge/waste. It is for its material robustness to chemical attack, mechanical stability, and excellent thermal and optical properties that we choose single crystal SiC as the base optical sensor material. There are numerous polytypes of SiC such as 3C (cubic), 2H (hexagonal), 4H (hexagonal), 6H (hexagonal) and 15R (rhombohedral). The key point to note is 6H-SiC's high 2500 °C melting temperature makes it ideal for extreme temperature conditions. In addition, its Young's elastic modulus, yield strength, and Poisson ratio prove it to be a mechanically robust material. These material properties make single crystal high thickness (e.g., 300 microns) 6H-SiC an ideal reliable candidate for extreme environment sensors such as coal-fired power plants. Finally, a sensor technology for any applications must be weight, size, and power consumption sensitive. The proposed solution indeed is favorable in these respects because (a) The frontend SiC chip is passive (uses no power), (b) the sensor uses low power (e.g., mW or less level) tunable laser (or two fixed wavelength low power lasers), (c) the sensor transceiver system only uses a few (e.g., 10) separate tiny chip scale components, (d) the sensor design is optically efficient and minimally invasive that helps packaging aspects. Most importantly, the sensor frontend capsule itself is completely passive and wireless allowing it to be utilized in

extremely harsh environments where standard electrical or optical wiring would not survive. Also, the proposed sensor design and signal processing eliminates effects of vibrations or beam misalignments making a practical sensor. Depending on the chip design and laser beam interrogation and signal processing, both temperature (T) and pressure (P) sensors can be realized in one compact unit.

Fig.1 shows the proposed hybrid sensor concept that uses a remotely placed all-passive optical sensor capsule made of single crystal SiC chip acting as the capsule window and a pressure sealed capsule assembly made of a suitable high pressure high temperature material such as a ceramic (including SiC forms, e.g., sintered SiC) or high pressure steel or alumina. The capsule has a high pressure connector that interfaces to the high pressure hot gas flow system that is linked to the high temperature high pressure hot gas flow system such as a fossil fuel plant under test. The SiC optical window sits in a specially designed sealed pressure seat that creates the desired high pressure boundary conditions for the deployed SiC chip.

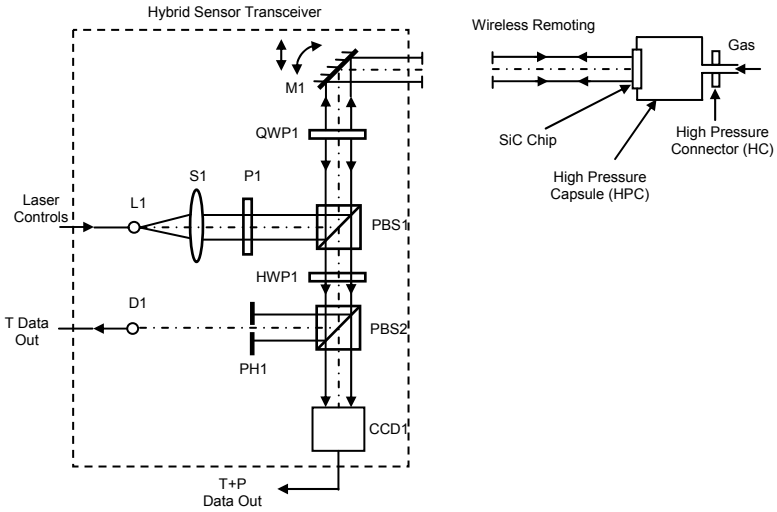

Fig.1 Proposed Wireless Hybrid Optical Sensor for Simultaneous Temperature and Pressure Measurements.

The Fig.1 sensor operates as follows. The input laser beam from the tunable laser L1 is expanded and collimated using spherical lens S1. The collimated beam then passes through a polarizer P1 to produce vertically or s-polarized light that is reflected off the cube polarization beam splitter PBS1. This reflected light then passes via a quarter-wave plate QWP1 to strike a beam alignment mirror M1. Hence circularly polarized light is directed towards the SiC chip window in the mounted capsule. M1 can be rapidly adjusted for tilts and translational motion to enable the beam to strike the SiC chip at normal incidence. The retro-reflected beam from the SiC chip retraces its path to produce a horizontal or p–polarized light beam that passes through PBS1 to strike a half-wave plate HWP1 that produces a linearly polarized beam at an angle of θ degrees with respect to the s-polarization direction. By controlling the rotation of the HWP1, the linear polarization angle θ can be changed to optimize the optical power split by the PBS2 that directs the sensed light beam to two independent light detection paths. The reflected beam enters a light path containing a pin-hole (PH1) that accepts only the on-axis rays from the SiC chip. After the pin-hole, a point detector D1 picks up the optical power from the selected on-axis rays. On the other-hand, the sensing straight beam passes through PBS2 to impinge on a two dimensional (2-D) optical detector array D2 such as a CCD chip. The rotation angle θ can be optimized to enable high detection signal-to-noise ratio (SNR) for both detectors.
Key principle of operations of the proposed sensor is the locally sensed interferometric cavity-type operation of a thick SiC chip in air for temperature assessment and the global sensing of the chip deformation due to pressure. The natural SiC crystal-Air interface produces a near 19% reflection of an incident beam (SiC index is 2.57 in 1550 nm IR band). Another 12.6% reflection occurs for the beam that travels through the crystal and returns to interfere with the first beam. Hence, the SiC chip in air forms a weak two beam etalon effect to produce light interference that can be used to measure temperature via a spatial local effect. This concept has been demonstrated in our earlier works [2-3, 5]. In Fig.1, this localized effect is captured by monitoring the on-axis central rays from the SiC chip. As the temperature changes, the SiC chip optical path length (OPL) changes dominated by the material refractive index change. By measuring this OPL change, the temperature of the chip can be measured. As pressure changes inside the

capsule (outside the capsule is 1 atm), the SiC chip deforms to produce a convex mirror effect. Note that only near the on-axis condition are the faces of the chip normal to the incident beam, hence producing true retro-reflection to create beams that pass via the pinhole to D1 to make the temperature-only measurement. In effect, as pressure (P) changes, the on-axis ray bundle remains essentially the same allowing a pressure independent temperature measurement. Here, the thick nature of the SiC single crystal chip helps reduce chip thickness changes due to pressure. Recall that the laser can be tuned to normalize the detected optical power values thus providing a self-calibration method. Note that using a thick (e.g., 300 microns) SiC chip improves the extreme environment operational robustness of the sensor front-end, thus improving the life-times of the overall sensor system. It is important to note that the SiC chip and chip seating in the capsule can be designed such that the out-of-plane deflection is mainly caused by internal pressure change with minimal contribution from temperature (T) effects. Such a design is possible by essentially using a chip packaging/boundary material with a similar Coefficient of Thermal Expansion CTE) to single crystal SiC. In this case, the differential CTE between the SiC chip and its boundary material becomes small such that the chip deflection is dominated by pressure changes versus temperature changes over the designed sensor operation range. Furthermore, post-processing of the acquired local and global optical power data can be used to isolate T and P measurements with extreme sensitivities.

As the pressure in the capsule increases with respect to the external pressure (e.g., 1 atm), the SiC chip assumes a convex mirror position for the striking incident collimating beam. In effect, the SiC convex mirror acts as a diverging refractive weak lens that produces a beam expansion for the reflected incident beam. The degree of this beam expansion depends on the distance between the SiC chip and the imager D2, the power of the weak lens, the optical wavelength, and the beam divergence properties of the SiC chip incident collimated beam. Thus by simply monitoring the size of the optical beam incident on the CCD image D2, one can essentially calculate the pressure experienced by the SiC chip in the capsule. In this case, it is assumed that temperature changes do not change the weak lensing power of the SiC convex mirror, and thus do not change detected beam size on the imager D2. This engineering assumption is possible as the high thermal conductivity of the SiC chip causes the given hot gas temperature to effect the chip globally and uniformly, thus preventing any thermal gradients on the chip spatial zone. Hence temperature will cause the same OPL change over the entire chip region. On the contrary, the pressure sealed boundary conditions for the mounted SiC chip dictates how the chip will deform due to the application of uniform pressure over the chip region. For a typical circular disk type design with the classic clamped edge or simply supported models, the SiC chip produces a convex mirror type deformation with maximum deflection at the center of the disk. Hence, one can assume that only pressure controls the extent of this convex mirror-type deformation. Thus the imaging magnification results from D2 can provide the sensed pressure data while the D1 provided normalized optical power data can provide the temperature data, hence forming the proposed hybrid temperature plus pressure wireless optical sensor. It is interesting to note that the previously mentioned description of hybrid sensor operation assumes a SiC chip with parallel front and back faces. Nevertheless, if the chip does not satisfy this condition exactly, the hybrid sensor is still operational. For instance, the two chip surfaces can have some fabrication limited profiles with a relative thickness variation. In this case, the retro-reflected beam observed by D2 will show a specific interference or fringe pattern due to the etalon like behavior of SiC in air. The key point to note is that as the pressure changes, the observed interference pattern does not change; only its size changes. On the other hand, when the chip temperature changes, the fringe pattern moves but the overall size of the pattern does not change. This observation of the proposed sensor can be used with advanced signal processing to make a high performance sensor that can deliver accurate and independent pressure and temperature readings. It is also important to note that for highly accurate temperature readings, the chip front and back surfaces should indeed be flat over that tiny local region of observation. In effect, the size and location of the pinhole can be optimized to get the best temperature sensitivity for a given SiC chip.

5. WIRELESS PRESSURE SENSOR DEMONSTRATION

In order to study the pressure measurement aspects of the proposed Fig.1 hybrid sensor, a high pressure capsule shown in Fig.2 is fabricated, assembled and then used in the Fig.3 wireless optical pressure sensor system set-up in the laboratory (see Fig.3 and Fig.4).

Fig.2. Close-up front-view of the experimental SiC chip mounted in the high pressure capsule.

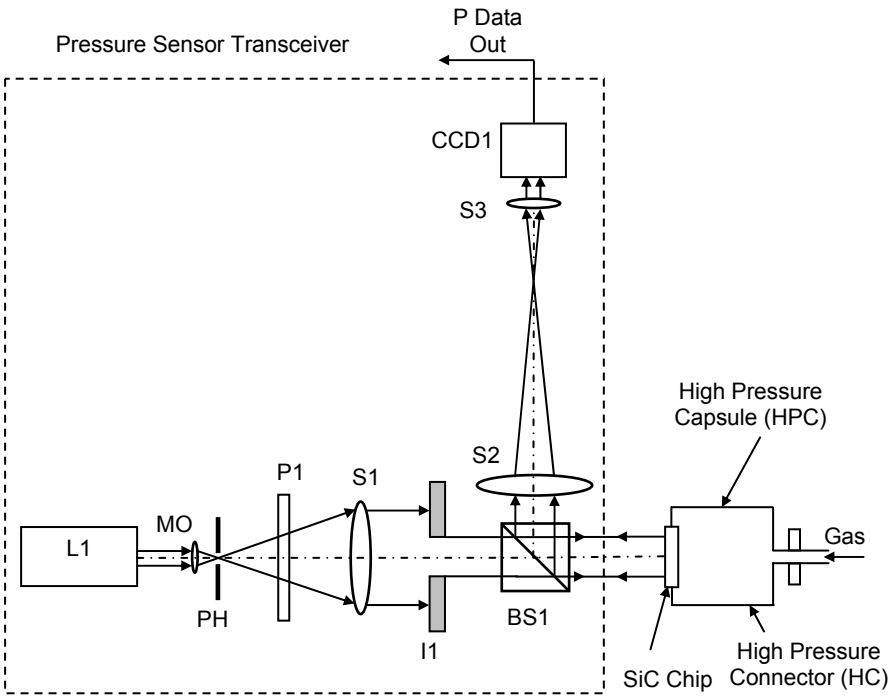

Fig.3. Proposed SiC-chip based wireless optical pressure sensor system test configuration.

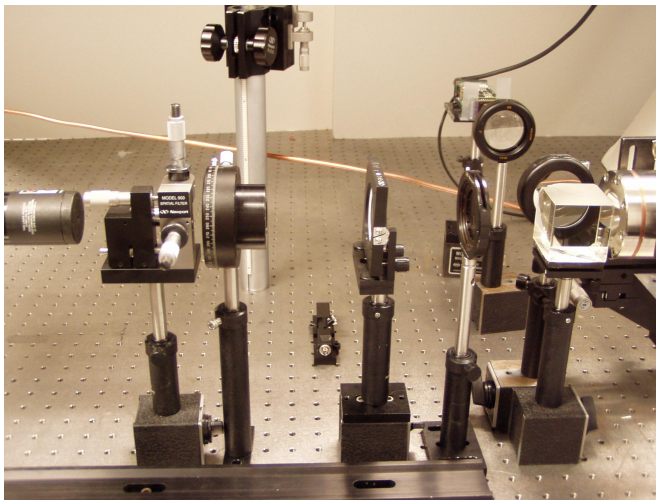

Fig.4 Experimental laboratory set-up for the SiC chip-based pressure sensor system.

To enable the Fig.3 experimental set-up, light from a 10 mW 633 nm HeNe laser source L1 is passed through an expansion-filter system of 10X microscope objective (MO) lens and 10 μm pin-hole (PH). The cleaned and expanded beam is collimated using a 15 cm biconvex lens S1. The beam is vertically polarized using a polarizer P1. The portion of the light beam that transmits through the Beam Splitter BS1 hits the SiC chip seated in the high pressure capsule with a sealed circular boundary of ~ 5 mm diameter. The 5 mm size of the beam hitting the SiC chip is controlled by an iris I1 placed between P1 and BS1. Under ambient atmospheric pressure conditions (1 atm ~ 1 bar), the reflection from the front and back surfaces of the SiC chip give a phase map that represents the relative optical path length differences between the two surfaces. This phase information is seen on a 2-D CCD detector CCD1 in the form of fringes. For a perfect flatness parallel faces chip, one would not observe any fringes; just a gray-scale uniform optical power level. The S2 and S3 imaging lenses used are 10 cm focal length lenses forming a 40 cm path 1:1 imaging system between the SiC chip and CCD. The temperature conditions during the experiment is the ambient 26 ºC room temperature. A compressed air cylinder is connected to the pressure capsule via a manual regulator to control the pressure inside the capsule relative to the external ambient 1 atm pressure.

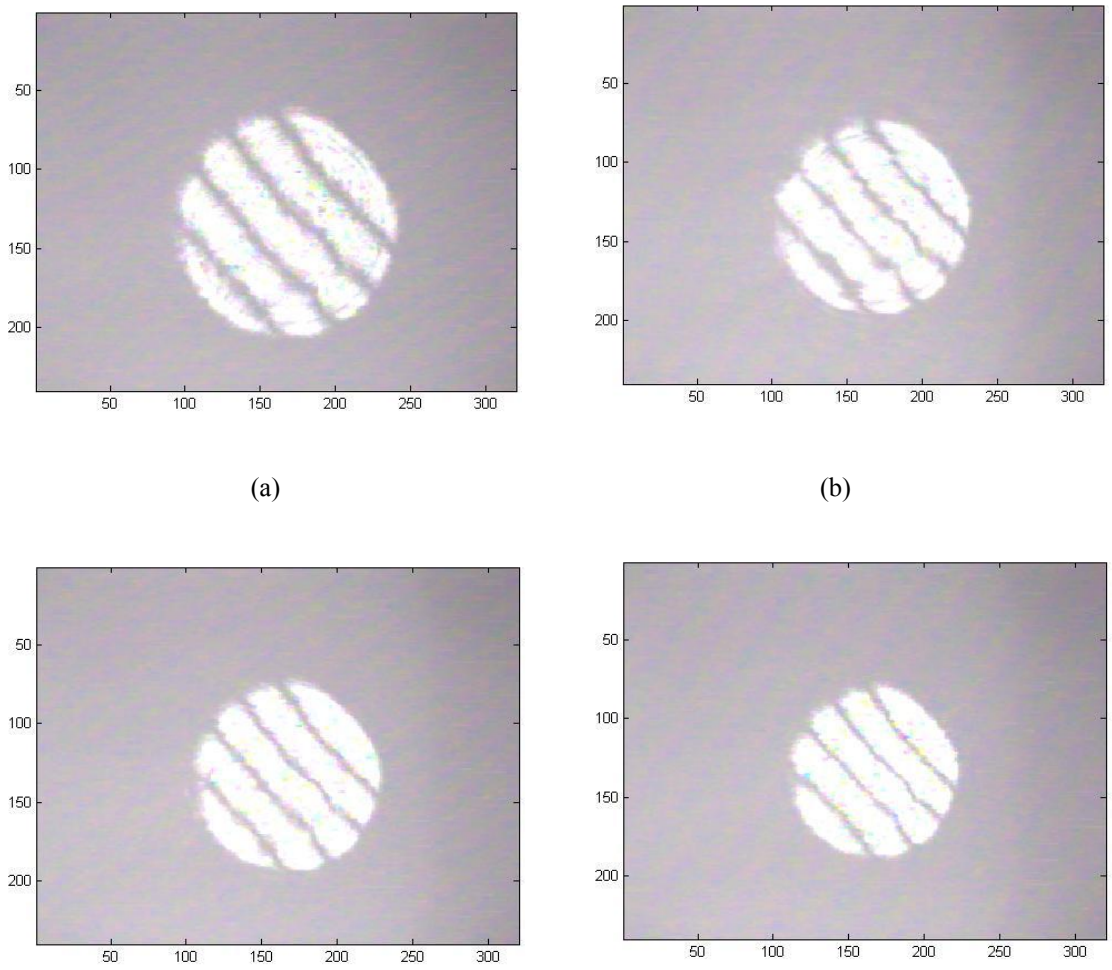

Fig.5. SiC chip-based pressure system $I_i(x,y)$ optical images produced for (a) 0 atm, (b) 13.6 atm (200 psi), (c) 27.2 atm (400 psi), and (d) 40.8 atm (600 psi) high differential pressure conditions in the pressure capsule. Axes: CCD pixel count.

The initial fringe pattern can be written as $I_i(x,y)$ as the initial phase map of a given SiC chip. This initial fringe pattern is seen in the Fig.5(a) photo produced by the CCD in the Fig.3 system when the pressure in the capsule is 1

atm and equal to the external pressure (hence differential pressure on SiC chip is zero). As the pressure is increased in the high pressure capsule above 1 atm, the SiC chip under small mechanical deformation conditions forms the proposed surface of a convex mirror to the incoming plane wavefront. Hence, one should expect a magnification of the beam received at the remote CCD. Compared to Fig.1, given the Fig.3 design uses a 1:1 imaging system between the chip and the CCD, the chip convex mirror-like deformation combined with the inverting imaging system produces a reduction in the beam size at the CCD. The initial SiC chip fringe pattern $I_i(x,y)$ has a 5 mm diameter when 1:1 imaged on-to the rectangular CCD plane. As shown in Fig.5, as the pressure in the capsule increases above 1 atm, the differential pressure P on the chip produces an increasing convex mirror chip deformation of the pattern $I_i(x,y)$ thus producing a pattern reduction in size. Fig.5 shows the set of images from the pressure sensor system where the initial fringe pattern size decreases with increasing capsule differential pressures up-to 40.8 atm (1 psi = 0.068 atm).

Table 1: Experimental Optical Image Size vs. Capsule Differential Pressure P

Differential Pressure P		Image Size	Measured Magnification
(psi)	(atm)	(CCD pixels)	(M=Image Size/147)
0	0	147	1.00
200	13.61	135	0.92
300	20.41	130	0.88
400	27.21	125	0.85
500	34.01	117	0.80
600	40.82	112	0.76

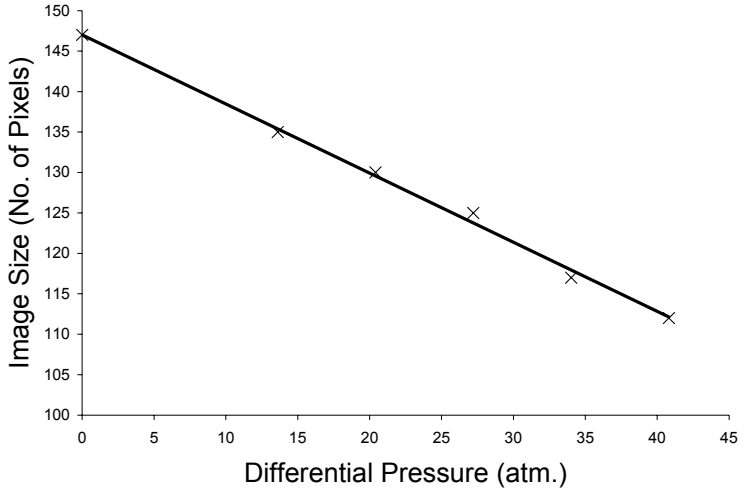

Fig. 6. Plot shows demagnification of incident beam size as it retro-reflects from the SiC chip under pressure acting as a weak convex mirror coupled to a 1:1 image inversion system.

A quantization of these image reduction versus applied differential pressure P in the capsule for P taken up-to 40.8 atm are shown in Table 1. Fig.6 connects the discrete experimental data to show a plot of differential pressure on SiC chip versus image size. These results show a linear behavior of the applied differential pressure versus the measured optical parameter of image size. Sensor pressure resolution is given by the inverse of the slope of the plot in Fig.6. This plot indicates a current experimental resolution of 1.17 atm calculated as 40.82 atm/ [(147-112) pixels]. Resolution measurement is restricted by the pixel size in the deployed CCD. Here 147 pixels of the CCD = 5 mm real size using the 1:1 imaging approach. One can greatly improve the pressure measurement resolution by decreasing the pixel size and increasing the size of the optical beam on the CCD plane. This is to our knowledge the

first demonstration of a wireless SiC optical chip for high pressure assessment and points to the robustness of the thick SiC chip under high gas pressures, a result needed for potential gas species detection using custom SiC chips.

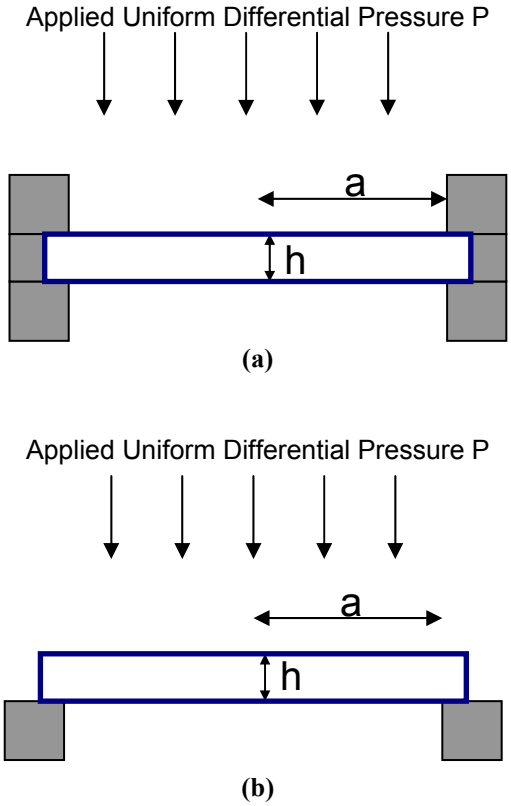

Fig. 7: Shown are the two Key Mechanical Models used to analyze the SiC Chip mechanical deformation behavior when seated in the proposed high pressure capsule. (a) Clamped Edge model and (b) Simply Supported model.

The mechanical response of the deployed 6H-SiC chip is dependant on its mounting in the given test pressure capsule. Specifically, the mounting method defines the boundary condition necessary for solving the equations that give the amount of deflection of the SiC chip which it turn determines the power of the pressure sensitive convex mirror behavior of the chip. Considering the design of the given pressure capsule SiC chip seat , two major methods, namely, a circular chip with 'Clamped Edges' and circular chip with 'Simply Supported Edges' are analyzed for the test capsule [see Fig.7(a),(b)]. In effect, the SiC chip experimental mounting method shown later in Fig.8 for the test capsule in this study results in a hybrid-solution of the above mentioned methods. Furthermore, the deflection analysis is sub-divided under two regimes of small and large deflection analysis. The small deflection regime is defined by the condition that the maximum deflection should be less than half the thickness of the chip [36]. Specifically, the region in the middle plane of the sensor chip, undergo small displacements perpendicular to the direction of the plane thus forming the middle surface of the chip. When these displacements are small in comparison with the thickness of the chip, the strain of the middle plate can be neglected and analysis is in the small deflection regime. When this is not true, the analysis is extended to include the effect of strain of the middle plane of the chip. This large deflection regime analysis gives deflection and stress results that deviate from the small deflection regime. As shown later via the experiments, the proposed pressure sensor operates well within the small deflection regime of the utilized 6H-SiC chip. Also note that failure stress analysis of the SiC chip is essential for a robust design. Hence, the maximum stress values generated for all pressure cases have to be evaluated. Proper design requires working with pressures that generate maximum stress values that are less than the failure yield stress value for 6H-SiC. This pressure-limited operation ensures the reliable and repeatable performance of the sensor chip and hence the optical sensor.

Fig.8 shows how the square 1 cm x 1 cm SiC chip is seated in the pressure capsule. The variable aperture seat (washer) used has a 5 mm diameter and creates the circular pressure boundary on the chip. The washer is attached to

the steel seat by a GE RTV 102 silicone rubber adhesive sealant with operational temperature range of – 60 °C to 204 °C. The SiC chip is attached to the washer using a layer of the same sealant. The sealant is filled in the canal of the brass seat so it strongly holds on to the steel seat. A layer of the sealant was also applied at the edges of the two seats to avoid any leaks. Fig.9 shows a snap shot of the actual seating hardware components, including a set of washers prepared for the experiment.

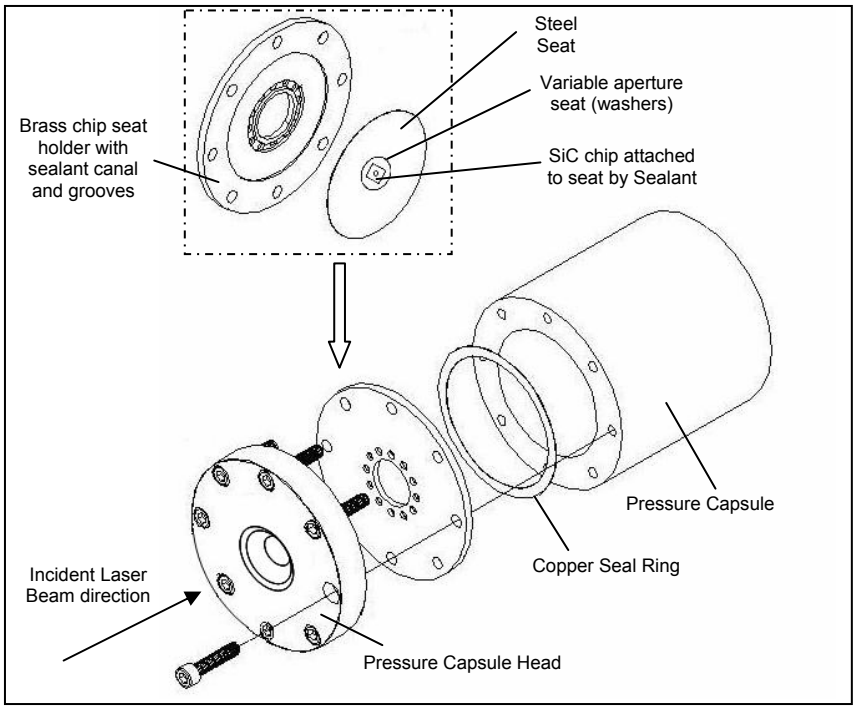

Fig.8. Experimental design used for seating the SiC chip in the high pressure capsule.

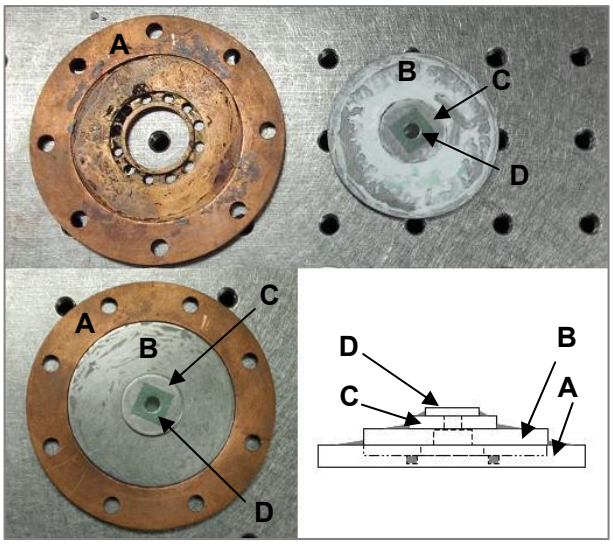

Fig.9. Snap shot of the experimental seating components and their arrangements used for seating the SiC chip in the high pressure capsule. Components in photograph are labeled as: A: Brass chip seat holder with sealant canal and grooves; B: Steel seat; C: Aperture seat (washer); and D: SiC chip.

Under uniformly distributed applied pressure the circular sensor chip with clamped edges (see Figure 7(a) exhibits deflection according to the following classic expression [37]:

$$w(r) = \frac{P}{64D}\left(a^2 - r^2\right)^2, \tag{4}$$

where *w(r)* is the bend in chip at a certain radius *r*, *P* is applied differential pressure between the two isolated sides of the chip, '*a*' is the radius of the chip, 'ν' is the Poisson's ratio and *D* is rigidity constant. *D* is defined as:

$$D = \frac{Eh^3}{12(1-\nu^2)}, \tag{5}$$

where *'E'* is the modulus of elasticity and '*h*' is the thickness of the chip. The maximum deflection is at the center of the chip and is given by:

$$w_{\max} = \frac{P}{64D}a^4. \tag{6}$$

The maximum stress caused by pressure is at the boundary of the chip given by the equation:

$$\left(\sigma_r\right)_{\max} = \frac{3Pa^2}{4h^2}. \tag{7}$$

For the circular sensor chip with supported edges (see Figure 7 (b)), the deflection under uniformly distributed applied pressure is given by the following expression [37]:

$$w(r) = \frac{P(a^2 - r^2)}{64D}\left(\frac{5+\nu}{1+\nu}a^2 - r^2\right). \tag{8}$$

The maximum deflection is at the center of the chip and is given by:

$$w_{\max} = \frac{Pa^4}{64D}\left(\frac{5+\nu}{1+\nu}\right). \tag{9}$$

The maximum stress in the supported chip caused by pressure is at the center of the chip given by the equation:

$$\left(\sigma_r\right)_{\max} = \frac{3Pa^2(3+\nu)}{8h^2}. \tag{10}$$

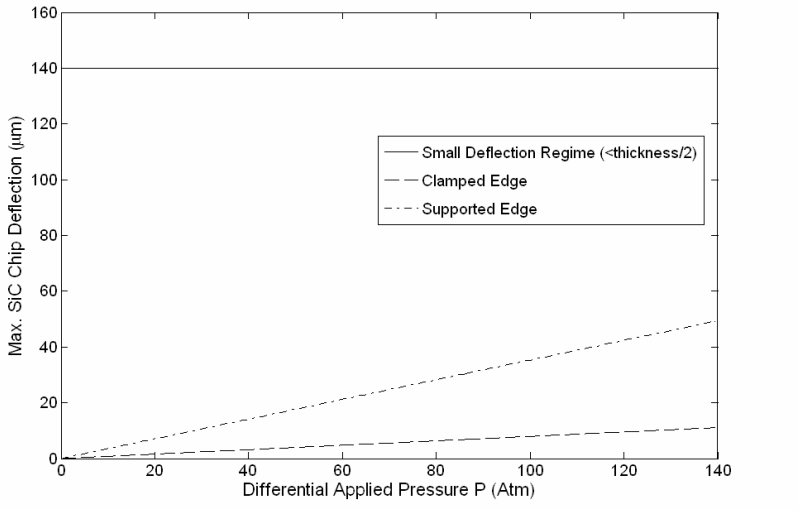

Fig. 10. Plot shows maximum SiC chip deflection 'w_{max}'(at the center of the chip) under applied pressure for the Clamped Edge and Supported Edge boundary condition models. The chip boundary diameter was taken to be 5 mm.

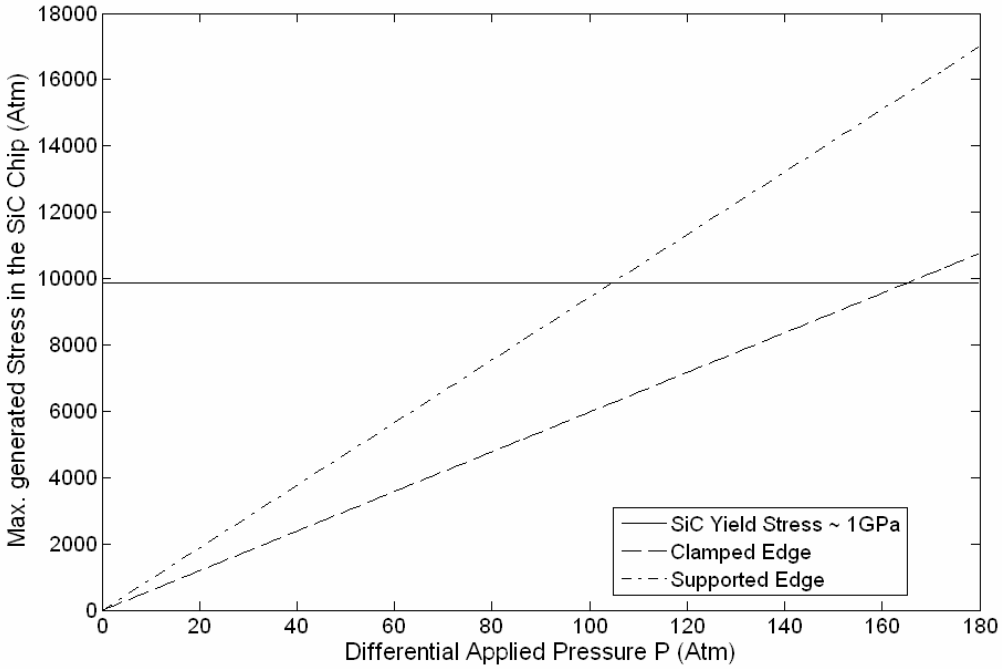

Fig.11.The expected stress produced in 6H-SiC sensor chip of 5mm diameter and 280 μm thickness.

Consider the experimental 6H-SiC chip with thickness *'h'* of 280 μm, radius *'a'* of 2.5 mm, Poisson's ratio *'v'* of 0.16 and Young's Modulus *'E'* of 415 GPa [38-39]. Fig.10 shows the expected deflection and Fig.11 shows the expected stress produced for this 6H-SiC sensor chip with the applied differential pressure as experienced in the pressurized capsule. Using a 1 GPa yield stress [40] (approx.) for the 6H SiC chip, the sensor chip and hence the sensor is expected to work safely up to a pressure of 100 atmospheres (atm). The maximum deflection of a 5 mm diameter pressure boundary sensor chip of thickness 280 μm is expected to be well within the small deflection range, [i.e. < Thickness/2= 140 μm], at 100 atmospheres. Comparing the two Fig.7 SiC chip seating setups in the small deflection regime, the supported edge chip seating case gives approximately 3.7~5 times larger deflection than the clamped chip case(see Fig. 10) but then it also gives 1.5~1.75 times higher maximum stress value (see Fig. 11). Since the experimental set-up to seat the SiC chip in the high pressure cell utilized in the study is a hybrid of the two cases, the maximum stress value is expected to be in a range whose limits are defined by the stress values given by the mentioned two cases. Same discussion holds true for the maximum deflection of the SiC chip. Note that in the large deflection regime, exact analytical solutions are not available and only approximate analytical solutions can be utilized. However, numerical methods and simulation tools (like Finite Element Method Software) can provide more exact solutions for the plate/chip deflections and stress values. The described experimental results indicate a SiC chip seating structure that is more clamped than supported, suggesting that the proposed sensor design is robust for pressures reaching ~140 atm (or 2058 psi). Geometrical analysis for weak lens/mirror optics (i.e., when lens/mirror radius of curvature R << Lens/mirror Central Thickness w_{max}) can be carried out to show that the SiC weak Convex Mirror focal length f_m in cm is given by:

$$f_m = \frac{R}{2} = \frac{{w_{\max}}^2 + a^2}{4 w_{\max} \times 10^4} cm, \qquad (11)$$

where w_{max} in microns is the SiC chip central position maximum displacement with applied differential pressure P and a is the radius in microns of the SiC chip pressure boundary. Using Equations 6, 9, and 11, and experimental pressure boundary of a= 2.5 mm, Table 2 gives the theoretically expected maximum chip central deflection and equivalent weak focal length values for the SiC chip under varying pressure values sustained in the experiment. Fig.12 shows the theory predicted focal length change for the SiC weak mirror for a broad range of pressures.

Table 2. Theoretical Central Deflections and Focal Lengths of the SiC Chip Convex Mirror versus Pressure.

Differential Pressure P		Model 1		Model 2	
		Supported Sensor Chip		Clamped Sensor Chip	
(psi)	(atm)	Chip Central Deflection w_{max} (μm)	Convex Mirror Focal Length f_m (cm)	Chip Central Deflection w_{max} (μm)	Convex Mirror Focal Length f_m (cm)
0	0	0.000	∞	0.000	∞
200	13.61	4.804	32.53	1.080	144.68
300	20.41	7.206	21.68	1.620	96.45
400	27.21	9.608	16.26	2.160	72.34
500	34.01	12.010	13.01	2.699	57.87
600	40.82	14.412	10.84	3.240	48.23

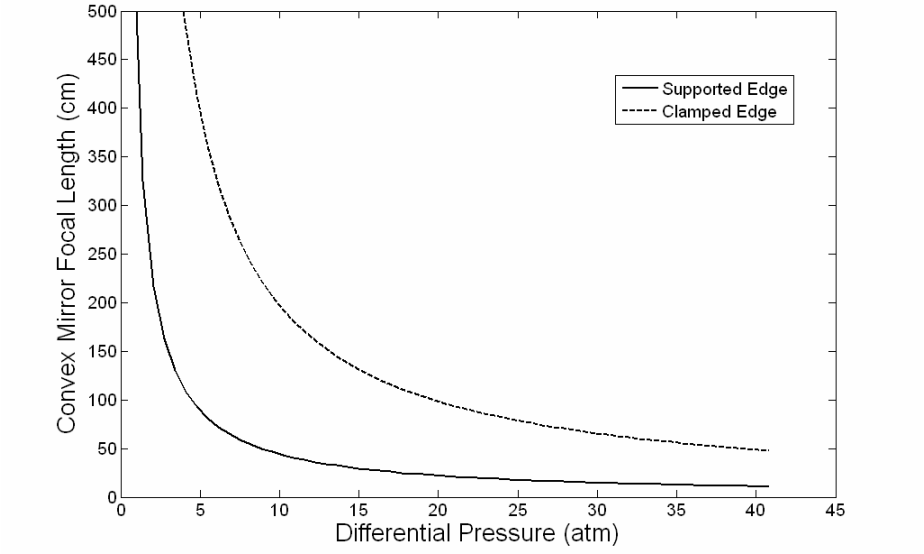

Fig. 12. Plot shows the effective theoretical focal length 'f_m' of the SiC chip acting as a convex mirror due to applied pressure. The focal length decreases as the differential pressure is increased.

Recall that the SiC chip acts as a weak convex mirror (equivalently, a weak concave lens) within the S1/S2 1:1 imaging system. Here, the S2 and S3 lenses have focal lengths F_2 and F_3, respectively. F_2= F_3=F=10 cm for the experiment. When the SiC chip experiences no differential pressure (P=0), it acts like a flat mirror and S3/S4 lenses form a 1:1 imaging system with magnification M=1. As P increases, the SiC chip starts acting like a convex mirror (or concave lens) with a long negative value focal length. It is well known that the equivalent focal length f_e from two lenses (one focal length F_2 and another focal length f_m) placed L apart is given by [41]:

$$f_e = \frac{F_2(L - f_m)}{L - (F_2 + f_m)}. \qquad (12)$$

Hence, the SiC chip weak concave lens in combination with the first imaging lens S2 (near the beam splitter in Fig.3) forms an equivalent imaging lens with a new f_n focal length. With F_2=F and L=F, and considering weak lensing conditions which are true for the proposed and tested SiC pressure sensor set-up, the new pressure dependent magnification M (or demagnification as f_m is a negative value) for the imaging system can be approximately written as:

$$M = \frac{F_3}{f_e} = \frac{F}{f_e} = \frac{f_m}{f_m - F} = \frac{1}{1 - F/f_m}. \qquad (13)$$

In the proposed experiment. F_3=F=10 cm and f_m has negative values as short as – 31.67 cm (at M=0.76). Using Eqn.13 and related experimental results, Table 3 gives a comparison for the expected and measured image magnification results for the demonstrated pressure sensor. Comparisons are made both with the clamped and supported models for the SiC seating in the pressurized capsule.

Table 3. Comparison of Experimental Demagnification with theoretical models.

Differential Pressure P		Demagnification M		
		Theoretical		Experimental
(psi)	(atm)	Supported	Clamped	
0	0	1	1.00	1.00
200	13.61	0.76	0.94	0.92
300	20.41	0.68	0.91	0.88
400	27.21	0.62	0.88	0.85
500	34.01	0.57	0.85	0.80
600	40.82	0.52	0.83	0.76

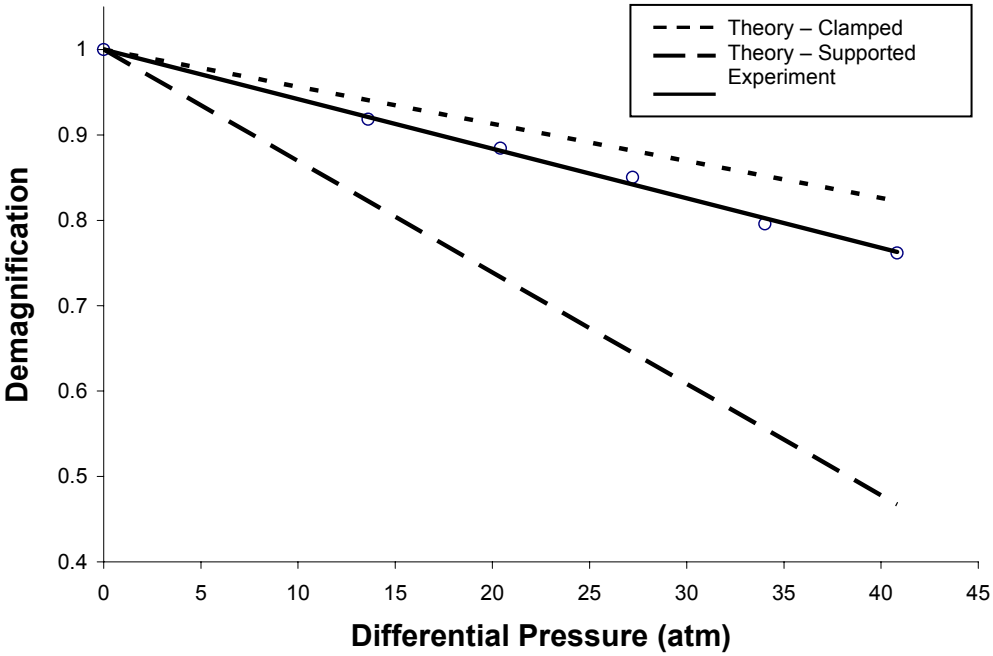

Fig. 13. Plot shows the experimental beam demagnification along with the theoretical demagnification for Clamped and Supported sensor chip models. The behavior of the chip shifts from clamped model towards supported model as the pressure increases.

Fig.13 shows the comparison plots for the detected image magnification versus pressure for the studied pressure sensor. Plots indicate the SiC seating closer to the clamped case, an expected results because of the pressure washer (seal) used to maintain the chip in a sealed arrangement.

5. CONCLUSION

A hybrid temperature plus pressure wireless sensor system has been proposed using a thick single crystal SiC chip seated in a pressure capsule and local and global spatial optical recognition. The concept has been tested as a pressure-only sensor up-to 41 atm. Initial experimental results show a linear mechanical and optical behavior of the SiC chip and sensor magnification parameter read-out indicating the robustness of the SiC chip technology under high pressures. Mechanical deflection analysis points to a clamped seating case for the SiC chip while stress analysis indicates a robust performance reaching 140 atm and beyond. The capsule requires coefficient of thermal expansion (CTE) matched designs such as using sintered SiC ceramics for packaging. These initial positive results attest to the promise and strengths of SiC chip based optical wireless sensor technology for fossil fuel based power generation system applications.

ACKNOWLEDGEMENTS

This paper was prepared with the support of the U.S. Department of Energy, under Award No. DE-FC36-03NT41923. However, any opinions, findings, conclusions, or recommendations expressed herein are those of the author(s) and do not necessarily reflect the views of the DOE. Support on the high pressure test capsule is provided by Applicote Assoc. (Dr. N. Quick). N. A. Riza is on part leave from UCF.

REFERENCES

[1] B. Culshaw, "Fiber-Optic Sensors: Applications and Advances," OSA Optics & Photonics News 16 (OPN 16), pp.24-29, Nov. 2005.

[2] N. A. Riza, M.A. Arain, and F. Perez, "Harsh Environments Minimally Invasive Optical Sensing Technique for Extreme Temperatures: 1000 °C and Approaching 2500 °C," International Conf. Proceedings of Optical Fiber Sensors 17 (OFS 17), SPIE Proc. Vol. 5855, pp.687-690, Bruges, Belgium, May 2005.

[3] N. A. Riza, M. A. Arain, and F. Perez, "Harsh Environments Minimally Invasive Optical Sensor using Freespace Targeted Single Crystal Silicon Carbide," to appear in IEEE Sensors Journal, Vol.6, June 2006.

[4] M. A. Arain and N. A. Riza, "Fiber Coupled In-Line heterodyne optical interferometer for Minimally Invasive Sensing," IEEE/OSA Journal of Lightwave Technology, Vol.23, No.8, pp.2449-2454, Aug. 2005.

[5] N. A. Riza, M. Arain, and F. Perez, " 6H- Single Crystal Silicon Carbide Thermo-Optic Coefficient Measurements for Ultrahigh Temperatures up-to 1273 K in the telecommunications infrared band," AIP Journal of Applied Physics, Vol.98, 103512, 2005.

[6] R.S. Okojie, A.A. Ned and A.D. Kurtz, "Operation of α(6H)-SiC Pressure Sensor at 500 ºC," IEEE International Conference on Solid-State Sensors and Actuators, pp. 1407-1409, Chicago, Illinois, Jun. 1997.

[7] R.S. Okojie, A.A. Ned and A.D. Kurtz, "Operation of *α(6H)*-SiC Pressure Sensor at 500 ºC," *Sensors Actuators A, Phys.*, Vol.66, No.1-3, pp.200-204, April 1998.

[8] R. Ziermann, J. von Berg, W. Reichert, E. Obermeier, M. Eickhoff and G. Krötz, " A High Temperature Pressure Sensor with β-SiC Piezoresistors on SOI Substrates," IEEE International Conference on Solid-State Sensors and Actuators, pp. 1411-1414, Chicago, Illinois, Jun. 1997.

[9] W. Pulliam, P. Russler, R. Mlcak, K. Murphy, and C. Kozikowski, " Micromachined SiC fiber-optic pressure sensors for high temperature aerospace applications," SPIE Proc. Vol.4202 on Industrial Sensing Systems, Ed. A. Wang and E. Udd, pp.21-30, Dec. 2000.

[10] A Dehennis, K.D. Wise, "A double-sided single-chip wireless pressure sensor," 15th IEEE International Conference on MEMS, pp. 252-255, Las Vegas, Nevada, Jan. 2002.

[11]O Akar, T Akin, and K Najafi, "A wireless batch sealed absolute capacitive pressure sensor," the 14th European Conference on Solid State Tranducers (EuorSensors), pp. 585-588, Copenhagen, Denmark, Aug. 2000.

[12] G Schimetta, F Dollinger, and R Weigel, "A wireless pressure-measurement system using a SAW hybrid sensor," IEEE Transactions on Microwave Theory and Techniques, Vol. 48, pp. 2730–2735, Dec. 2000.

[13] MA Fonseca, JM English, M von Arx, MG Allen, "Wireless micromachined ceramic pressure sensor for high-temperature applications," Journal of Microelectromechanical Systems, Vol. 11, pp. 337-343, 2002.

[14] C. E. Lee and H. F. Taylor, "Sensors for smart structures based on the Fabry-Perot interferometer," Chapter 9, pp. 249-270, Fiber Optic Smart Structures, Ed. Eric Udd, New York: Wiley, 1995.

[15] R. Duncan, D. Gifford, V. Rajendran, “OFDR tracks temperatures on power generators,” Laser Focus World Magazine 39:1010, pp. 89-92, p.89, Oct. 2003.
[16] A. D. Kersey, M.A. Davis, H.J. Patrick, M. LeBlanc, K.P. Koo, C.G. Askins, M.A. Putnam, E.J. Friebele, “Fiber Grating Sensors,” IEEE/OSA Journal of Lightwave Technology, Vol.15, No.8, pp.1442-1463, Aug. 1997.
[17] B. Culshaw, “Optical Fiber Sensor Technologies: Opportunities and Perhaps Pitfalls,” IEEE/OSA Journal of Lightwave Technology, Vol. 22 , No. 1, pp 39 – 50, Jan. 2004.
[18] L. Tenerz, L. Smith, and B. Hök, “ A Fiber Optic Silicon Pressure Microsensor for measurements in Coronery Arteries,” in Proc. Sixth Int. Conf. on Solid State Sensors and Actuators, Digest of Technical Papers Transducers’91, pp. 1021-1023, San Francisco, California, , 1991.
[19] R. A. Wolthuis, G. L. Mitchell, E. Saaski, J. C. Harti, and A. Afromowitz, "Development of medical pressure and temperature sensors employing optical spectrum modulation," IEEE Transactions on Biomedical Engineering. Vol. 38, pp. 974-981, 1991.
[20] Y. Kim and D. P. Neikirk, "Micromachined Fabry-Perot cavity pressure transducer," IEEE Photonics Technology Letters Vol. 7, No. 12, pp. 1471-1473 (1995).
[21] J. Han, J. Y. Kim, T. S. Kim, and J. S. Kim, "Performance of Fabry-Perot microcavity structures with corrugated diaphragms," Sensors Actuators A, Vol. 79, pp. 162-72 (2000).
[22] T. Katsumata, Y. Haga, K. Minami and E. Esashi, “Micromachined 125 □m Diameter Ultra-Miniature Fiber-Optic Pressure Sensor for Catheter,” Trans. Inst. Electr. Eng. Jpn. Part E, Vol. 120-E, pp. 58-63, 2000.
[23] J. Zhou, S. Dasgupta, H. Kobayashi, J.M. Wolff, H.E. Jackson and J.T. Boyd, “ Optically interrogated MEMS pressure sensors for propulsion applications,” Optical Engineering, Vol. 40, pp. 598-604, 2001.
[24] D.C. Abeysinghe, S. Dasgupta, J.T. Boyd and H.E. Jackson, “A novel MEMS pressure sensor fabricated on an optical fiber, IEEE Photonics Technology Letters, Vol. 13, pp. 993-995, 2001.
[25] W. Li, D. C. Abeysinghe, and J. T. Boyd, “Wavelength Multiplexing of microelectromechanical system pressure and temperature sensors using fiber Bragg gratings and arrayed waveguide gratings,” Optical Engineering, Vol. 42, 2, pp.431-438, Feb. 2003.
[26] W. J. Wang, R. M. Lin, D. G. Guo, and T. T. Sun, "Development of a novel Fabry-Perot pressure microsensor," Sensors and Actuators A, Vol. 116, Issue 1, pp. 59-65, Oct. 2004.
[27] W. Li, D. C. Abeysinghe, J. T. Boyd, “Multiplexed sensor system for simultaneous measurement of pressure and temperature,” Optical Engineering, Vol. 43, 1, pp.148-156, Jan. 2004.
[28] D Guo, W. Wang, R Lin, “Theoretical analysis and measurement of the temperature dependence of a micromachined Fabry-Perot pressure sensor,” Applied Optics, Vol. 44, Issue 2, pp. 249-256, Jan. 2005.
[29] Y. Zhu, A. Wang, “Miniature fiber-optic pressure sensor,” IEEE Photonics Technology Letters, Vol. 17, Issue 2, pp. 447-449, Feb. 2005.
[30] J. Xu, G. Pickrell, X. Wang, W. Peng, K. Cooper, A. Wang, “A novel temperature insensitive optical fiber pressure sensor for harsh environments,” IEEE Photon. Tech. Lett., Vol.17, No. 4, pp. 870-872, 2005.
[31] D. Donlagic and E. Cibula, “All-fiber high sensitivity pressure sensor with SiO2 diaphragm,” Optics Letters, Vol.30, Issue16, pp. 2071-2073, Aug. 2005.
[32] H. Xiao, J. Deng, Z. Wang, W. Huo, P. Zhang, M. Luo, G. Pickrell, R. May, and A. Wang, “Fiber optic pressure sensor with self-compensation capability for harsh environment applications,” Optical Engineering, Vol.44, Issue 5, 054403, May 2005.
[33] M. Li, M. Wang, and H. Li, "Optical MEMS pressure sensor based on Fabry-Perot interferometry," Optics Express, Vol. 14, Issue 4, 1497-1504, Feb. 2006.
[34] Y. Zhu, K. L. Cooper, G. R. Pickrell, and A. Wang, “ High-Temperature Fiber-Tip Pressure Sensor,” IEEE/OSA Journal of Lightwave Technology, Vol. 24, No.2, pp. 861 – 869, Feb. 2006.
[35] P. Fairley, “The Greening of GE,” IEEE Spectrum, pp.28-33, July 2005.
[36] J. H. Ausubel, “Big Green Energy Machines,” The Industrial Physicist, AIP, pp.20-24, Oct./Nov., 2004.
[37] S. P. Timoshenko and S. Woinowsky-Krieger, Theory of Plates and Shells, Chapter 2, Pure Bending of Plates, pp. 56-57, (McGraw-Hill Inc., New York, NY 1959).
[38] NIST Structural Ceramic Data Base, SRD Data Base No.30. (www.ceramics.nist.gov/srd/summary/scdscs.htm)
[39] R. G. Munro, “Material properties of a Sintered alpha-SiC,” Journal of Physical and Chemical Reference Data, Vol. 26, pp. 1195-1203, 1997.
[40] Sharpe W.N., Jadaan O., Beheim G.M., Quinn G.D., Nemeth, N.N., “Fracture Strength of Silicon Carbide Microspecimens,” IEEE Journal of Microelectromechanical Systems, Vol. 14, No. 5, pp. 903 – 913, Oct. 2005.
[41] E. Hecht, Optics, p.148, Eqn.5.36, 2nd Edition, Addison-Wesley, Reading, MA, 1990.